An inertia compensation scheme of wind turbine simulator considering time delay for emulating large-inertia turbines

Minghui Yin[1*], Weijie Li [1], C.Y. Chung [2], Zaiyu Chen [1], Yun Zou[1]

[1] The School of Automation, Nanjing University of Science and Technology, Nanjing 210094, China
[2] The Department of Electrical and Computer Engineering, University of Saskatchewan, Saskatoon, SK S7N 5A9 Canada
[*] ymhui@vip.163.com

Abstract: Wind turbine simulators (WTS), devised for pre-validation of control strategies for wind energy conversion system, commonly employ the inertia compensation scheme for reproducing mechanical behaviours similar to real wind turbines (WT). However, it is found in this paper that when a WT with large inertia is simulated, the time delay in command communication from control unit to motor driver, usually neglected in the existing inertia compensation scheme, results in the oscillating acceleration response and consequently leads to instability of the WTS system. As a result, the existing WTS is unable to stably simulate large-inertia WTs, which significantly limits its applicability. Hence, in this paper, a linear discrete model of the inertia compensation part that considers time delay of acceleration observation and communication is developed. Based on this model, an improved inertia compensation scheme in which a high-order filter is introduced to eliminate the deviation of acceleration response caused by the two types of time delay, is proposed. Finally, the improved inertia compensation scheme and its applicability to simulating a 600kW CART3 WT developed by National Renewable Energy Laboratory (NREL) are experimentally verified.

1. Introduction

Design and investigation of advanced wind turbine control strategies has become a hot issue in recent years. For preliminary validation of innovative algorithms of wind energy conversion system (WECS), wind turbine simulator (WTS) has become a necessary tool for research laboratories because field experiments are quite difficult and costly.

The slow response of wind turbine (WT) to wind speed fluctuation is caused by its high rotor inertia. Since this exerts a significant influence upon the design and operation of control strategies in WECS, such as maximum power point tracking (MPPT) control [1, 2] and active power control [3], the WTS should replicate the mechanical behavior of a real WT [4-7]. However, because the moment of inertia of WTS (denoted by J_s) is much smaller than the one for emulating WT dynamics (denoted by J_t), an inertia compensation scheme is usually implemented in WTS to simulate the slow mechanical behavior of a real WT [6-8].

Stability is necessary for a practical WTS. However, it has been revealed that when simulating real turbines with high rotor inertia, the WTS with the inertia compensation scheme is unstable, resulting in the oscillation of compensation torque [4-7]. To avoid instability, the ratio of J_t to J_s (J_t / J_s) should be less than a critical value, which is proved to be 2.0 when applying the conventional inertia compensation

strategy [4]. Therefore, the maximum inertia of WTs that can be stably emulated is significantly reduced by instability and accordingly the applicability of WTS to simulating large-inertia WTs is greatly limited.

It is intuitively pointed out that the high frequency noise of speed measurement results in torque oscillation [6, 7]. Accordingly, a low-pass filter (LPF) is utilized to eliminate the interfering signals [6, 7]. The similar LPF for filtering out external noise is also proposed in [8] and 9]. Furthermore, the pseudo derivative feedback [10] and estimation of the load torque [11] are developed to avoid the differential-based acceleration observation which easily exaggerates external noise of speed measurement. These methods focus on improving the acceleration observation by removing differentiator, which, however, increases the complexity of implementation.

Furthermore, by establishing a linear discrete model of WTS considering the discrete process of acceleration observation, the cause of WTS instability is interpreted as the one-step time delay of differential-based acceleration observation [4, 5]. On this basis, an inertia compensation scheme with a first-order filter added in the torque compensation loop is proposed to stabilize WTS without changing the inner loop control and experimental hardware.

However, it is experimentally found in this paper that the delay in communication from control unit to executive motor driver has a considerable effect on the stability of WTS and consequently reduces the critical value of J_t / J_s. Due to the small moment of inertia of the WTS test rig, the control cycle of WTS is usually set within tens of milliseconds to ensure sufficient control bandwidth [12]. In this case, the communication delay, usually neglected in the existing inertia compensation schemes, is comparable with the control cycle. Hence, the communication delay and its effect on the stability of WTS should be carefully modeled in the design of inertia compensation scheme.

In this paper, the inertia compensation part is extracted from WTS system and modeled as a linear difference equation with consideration of time delay of acceleration observation as well as communication delay. Based on this model, stability of the inertia compensation part is investigated through the time-domain response analysis method and an unexpected deviation response caused by time delay is derived. To overcome the limitation of simulating large-inertia WT caused by the WTS instability, an improved inertia compensation scheme is proposed, with a high-order filter added in the compensation loop. Its parameters are determined by pole assignment to eliminate the deviation response and increase the critical value of J_t / J_s. Finally, the improved inertia compensation scheme and its applicability to simulation of the NREL (National Renewable Energy Laboratory) CART3 wind turbine [13] are experimentally validated.

The remainder of the paper is organized as follows. Section II briefly describes the model of WTS

and the inertia compensation scheme. The inertia compensation part is extracted from WTS system and its discrete linear model considering time delay is developed in Section III. In Section IV, the stability condition of the inertia compensation part is analyzed and the improved inertia compensation scheme based on a high-order filter is proposed. In Section V, experimental studies on the WTS with the improved inertia compensation scheme are carried out. Finally, the conclusion is drawn.

2. WTS and the inertia compensation scheme

In this section, the configuration of WTS is introduced and the model of WTS including inertia compensation scheme and scaling transform is reviewed. It should be pointed out that because this paper aims to stably replicate the slow dynamic behavior of large-inertia WTs, a simplified WT model neglecting blade elasticity and shaft torsion is employed. This implies that the aeroelastic behavior and structural vibration of WTs, which are also relevant to the turbines' control strategies, cannot be mimicked by the WTS developed in this paper.

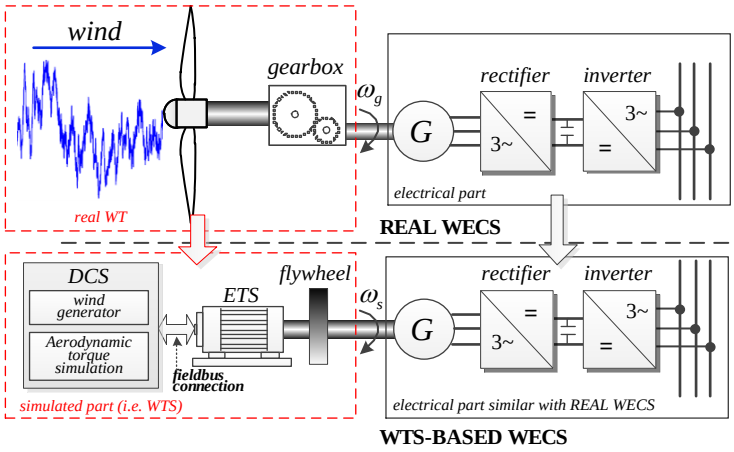

Fig. 1. *Comparison of the WTS-based WECS and real WECS.*

2.1. Structure of the WTS

As illustrated in Fig. 1, a WTS-based WECS is commonly divided into two parts, the simulated part and the electrical part [12]. The simulated part, i.e. the WTS system, is to replace the real WT. And, the electrical part, whose hardware implementation is similar with that of real WECS, includes the generator and its grid-connected convertor implemented with the investigated control strategy, such as MPPT control.

The WTS system mainly consists of two subsystems: a real-time digital control system (DCS) and a high-performance electromechanical tracking system (ETS). The DCS is embedded with aerodynamic theory of WT and wind generator, and the ETS carries out the torque control execution.

To describe the aerodynamics, the output torque of the wind rotor is usually given by:

$$T_a = 0.5\rho\pi R^2 v^3 C_p(\lambda)/\omega_r \tag{1}$$

$$\lambda = \omega_r R/v \tag{2}$$

where v is wind velocity, ρ is air density, R is radius of wind turbines, ω_r is rotor speed, and C_p is power coefficient which is a nonlinear function of tip speed ratio λ.

2.2. Modeling of the WTS with conventional inertia compensation scheme

According to Fig. 1, the mechanical dynamics of a real WT is usually represented as two rigid bodies (namely a wind rotor with large inertia J_r and a generator with small inertia J_g) linked by a flexible shaft and an ideal gearbox with gear ratio n_g [1, 2], i.e.,

$$\begin{cases} J_r\dot{\omega}_r + D_r\omega_r = T_a - T_{ls} \\ J_g\dot{\omega}_g + D_g\omega_g = T_{hs} - T_g \\ T_{ls} = K_{ls}\left(\theta_r - \theta_{ls}\right) + D_{ls}\left(\omega_r - \omega_{ls}\right) \\ n_g = \dfrac{T_{ls}}{T_{hs}} = \dfrac{\omega_g}{\omega_{ls}} = \dfrac{\theta_g}{\theta_{ls}} \end{cases} \tag{3}$$

where ω_r, ω_g are rotor and generator speed, T_a, T_g are aerodynamic torque and generator (electromagnetic) torque, T_{ls}, T_{hs} are low-speed and high-speed shaft torque, D_r, D_g are rotor and generator external damping, K_{ls}, D_{ls} are low-speed shaft stiffness and damping, and θ_r, θ_{ls}, θ_g are angular deviations on rotor-side, gearbox-side and generator-side.

If a perfectly rigid low-speed shaft is assumed, the mechanical dynamics of a real WT can be further represented as a single lumped mass model (on the generator-side):

$$J_w\dot{\omega}_g + D_w\omega_g = T_a / n_g - T_g \tag{4}$$

where $J_w = J_r / n_g^2 + J_g$ and $D_w = D_r / n_g^2 + D_g$.

Similarly, the mechanical behaviors of the WTS test bench can be expressed by:

$$J_s\dot{\omega}_s + D_s\omega_s = T_s - T_{sg} \tag{5}$$

where ω_s is rotational speed of the WTS, T_s is simulated torque of the WTS, J_s, D_s are total inertia and total damping of the test bench, and T_{sg} is generator torque of the test bench.

Because of the huge difference of inertia and power capacity between the WTS and real WT, T_s cannot be simply regulated according to T_a / n_g. To simulate the mechanical dynamics of a megawatt-scale WT with large inertia, the kilowatt-scale WTS usually employs an inertia compensation scheme [6-8] and

scaling transform [12]. Firstly, scaling down (4) by a factor of n_s that satisfies $T_{sg} = T_g / n_s$ yields a scaled-down WT:

$$J_t \dot{\omega}_g + D_t \omega_g = \frac{T_a}{n_g n_s} - \frac{T_g}{n_s}. \tag{6}$$

Here, $J_t = J_w / n_s$ and $D_t = D_w / n_s$ are the inertia and damping of the scaled-down WT, respectively. Note that the scaled-down WT is equated with the real WT (hereinafter collectively referred to as WT), because the mechanical dynamics represented by (4) and (6) are identical. Then, subtracting (6) from (5) with the assumption that ω_s is equal to ω_g and the rearrangement gives:

$$T_s = \frac{T_a}{n_g n_s} - \left(D_t - D_s\right)\omega_s - \left(J_t - J_s\right)\dot{\omega}_s \tag{7}$$

where $\left(J_t - J_s\right)\dot{\omega}_s$ and $\left(D_t - D_s\right)\omega_s$ are defined as the inertia compensation torque T_{comp} and damping compensation torque, respectively. Thus, by applying (7), as depicted in Fig. 2, modelling of WTS with the conventional inertia compensation scheme and scaling transform is as follows:

$$J_s \dot{\omega}_s + D_s \omega_s = \frac{T_a}{n_g n_s} - \left(D_t - D_s\right)\omega_s - \left(J_t - J_s\right)\dot{\omega}_s - \frac{T_g}{n_s}. \tag{8}$$

If T_s can be precisely calculated and controlled by (7), the rotational speed of WTS is equal to WT and accordingly, the mechanical dynamics of the two systems are identical. Note that scheme (7) is designed within a continuous time domain.

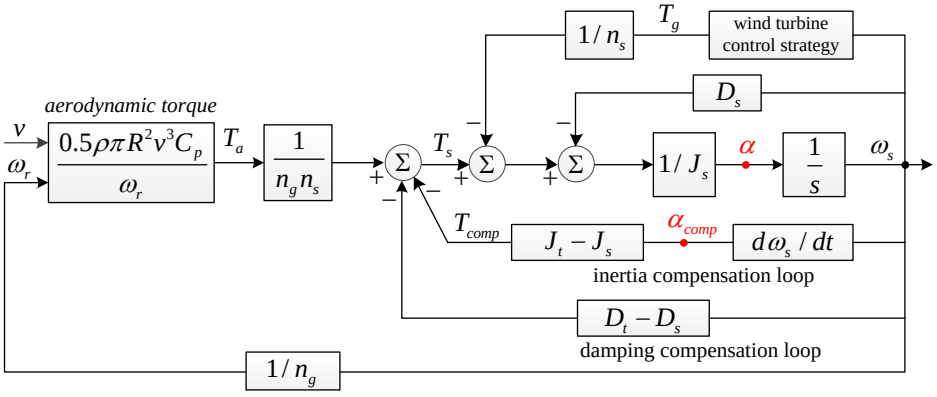

Fig. 2. *Block diagram of WTS system with the conventional inertia compensation scheme and scaling transform.*

3. Discrete model of inertia compensation part of WTS considering time delay

Because it takes time to gather operating data and execute control algorithm and command, systems often operate with various degrees of delay which might cause system instability or degradation of operations performance [14, 15]. In this section, two types of time delay are introduced and a discrete model is developed considering delays in inertia compensation part of WTS.

3.1. Time delay of acceleration observation

In the conventional inertia compensation scheme, it is assumed that the varying rotational acceleration can be obtained precisely and instantly. Actually, rotational acceleration can hardly be measured directly [16]; it is estimated through the difference in adjacent rotational speeds measured via optical encoder [4-7, 10]. Therefore, the scheme based on continuous time domain has to be digitalized in the real-time DCS [5] and the corresponding acceleration in the compensation loop is calculated by:

$$\alpha_{comp}(k) = \frac{\omega_s(k) - \omega_s(k-1)}{\Delta t} \tag{9}$$

where Δt is the control cycle of the real-time DCS. Likewise, the integral element is discretized:

$$\omega_s(k+1) = \omega_s(k) + \alpha(k) \cdot \Delta t \tag{10}$$

where $\alpha(k)$ is the average acceleration between two successive sampling points, i.e. $k\Delta t$ and $(k+1)\Delta t$. Substituting (10) into (9), acceleration in the compensation loop is actually calculated by [5]:

$$\alpha_{comp}(k) = \alpha(k-1). \tag{11}$$

It is obvious that a one-step time delay is inevitable in the discretization process of inertia compensation loop. Note that this type of time delay is irrelevant to the speed sampling interval and it always exists.

3.2. Communication time delay

In the WTS system showed in Fig. 1, the DCS communicates with the ETS via fieldbus connection and transmission of control variables, e.g. the executed torque, is to some extent delayed. Besides, due to the small moment of inertia of the WTS test rig and the resulting fast transient response, tiny control cycles are necessary to ensure sufficient control bandwidth [12], which makes communication delay more pronounced. Furthermore, as demonstrated in Section 5, this paper reveals that the communication delay, usually neglected in the existing inertia compensation schemes, has a considerable effect on the stability of WTS. Therefore, in this paper, the communication delay is modeled as a constant value:

$$\tau = k_0 \cdot \Delta t \tag{12}$$

where τ is the communication time delay, k_0 is the number of discrete delay steps.

3.3. Discrete model of inertia compensation part of WTS with time delay

Considering the aforementioned two types of time delay, the WTS system (Fig. 2) is remodeled (Fig. 3(a)). Based on the simulation and experimental observation that the oscillation of the inertia

compensation torque plays a predominant role in the variation of T_s when the WTS with conventional inertia compensation scheme is unstable, it is reasonable to suppose that the inertia compensation part (enclosed within the dashed line shown in Fig. 3(a)) is responsible for the WTS instability. Therefore, the inertia compensation part, in which the imbalance torque ΔT and the acceleration α are regarded as the input and output respectively, is extracted to examine whether this part can result in additional risk of WTS instability. Correspondingly, the inertia part is extracted from the discrete model of the WT system for comparison analysis, as shown in Fig 3(b).

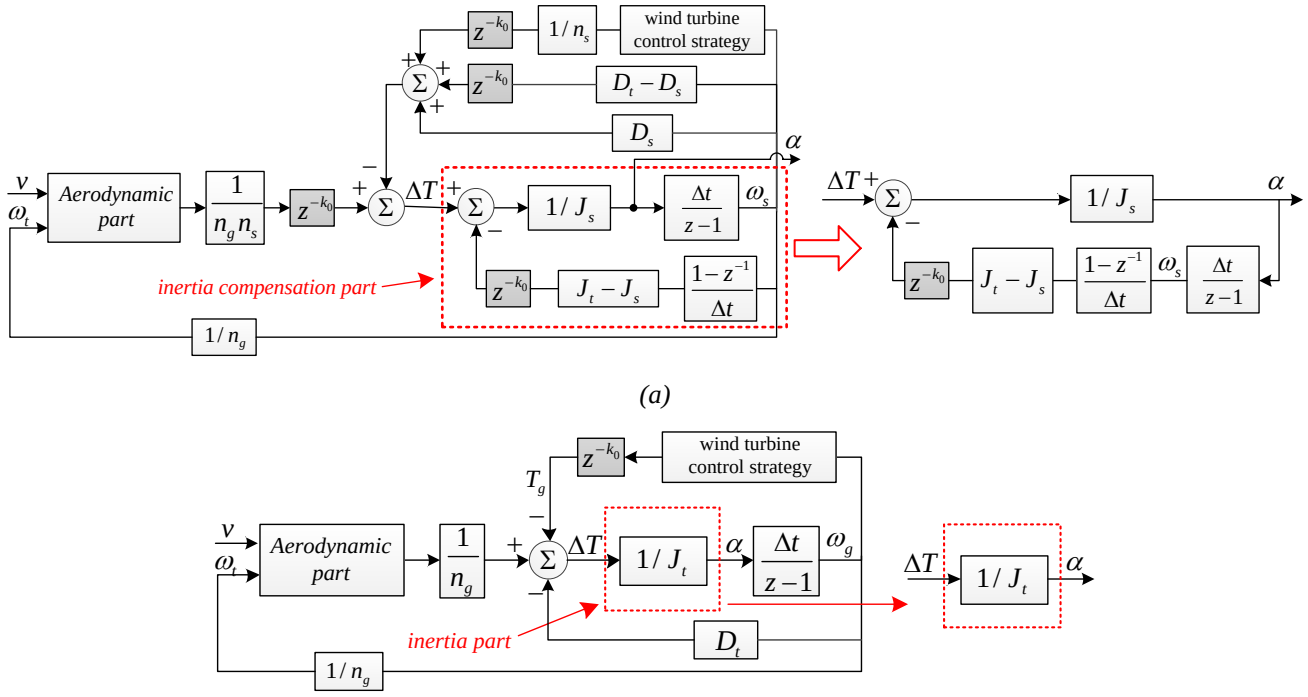

Fig. 3. *Discrete models of WTS system and WT system.*
(a) Discrete models of WTS system considering two types of time delay and inertia compensation part.
(b) Discrete models of WT system and inertia part.

Then, a linear difference equation with constant coefficients that describes the inertia compensation part of WTS system is given as:

$$\alpha(k)=\frac{J_s-J_t}{J_s}\cdot\alpha(k-k_0-1)+\frac{1}{J_s}\cdot\Delta T(k) \tag{13}$$

Correspondingly, the inertia part of WT system is as follows:

$$\alpha(k)=\frac{1}{J_t}\cdot\Delta T(k) \tag{14}$$

By comparing (13) with (14), it is seen that if the k_0+1 steps of state time delay caused by the delay in acceleration observation and communication is removed, the inertia compensation part of WTS becomes entirely consistent with the inertia part of WT.

It is worth noting that precisely because the complex nonlinear aerodynamic part and wind turbine control strategy are neglected in the linear model (13), the difficulty of stability analysis of WTS is substantially reduced and correspondingly the classical time-domain and frequency-domain analysis methods can be utilized to analyze the WTS stability and improve the inertia compensation scheme.

4. Improved inertia compensation scheme based on high-order filter

In this section, stability of the inertia compensation part is investigated based on time-domain response analysis and frequency-domain analysis. The deviation response of WTS's inertia compensation part characterized by fluctuation and divergence is derived, based on which, a high-order filter is proposed to mitigate the deviation response. Thus, the inertia compensation part of WTS is stabilized and its time-domain response remains in accordance with the inertia part of WT.

4.1. Response analysis on the inertia compensation part of WTS

Firstly, the influence of the two types of time delay on stability of the inertia compensation part is analyzed by the z-transform theory. According to (13), the z transfer function of the inertia compensation part of WTS is derived as:

$$G_{wts}(z)=\frac{1}{J_s z^{k_0+1}+J_t-J_s}. \tag{15}$$

It can be inferred from (15) that

1) If $\left|(J_s-J_t)/J_s\right|<1$, i.e., $J_t/J_s<2$, the poles of (15) locate inside the unit circuit in z plane and the inertia compensation part of WTS is stable;

2) If $J_t/J_s>2$, the inertia compensation part of WTS is unstable.

Then, to elaborate on this stability condition, the time domain response of inertia compensation part and inertia part excited by a step input of $\Delta T=u(k)$ is derived according to (13) and (14), respectively:

$$\alpha_{wts}(k)=\alpha_{wt}(k)+\alpha_d(k)=\frac{1}{J_t}\cdot u(k)-\frac{1}{J_t}\cdot m^N\cdot u(k)\ ,N=\left[\frac{k}{k_0+1}\right] \tag{16}$$

$$\alpha_{wt}(k)=\frac{1}{J_t}\cdot u(k) \tag{17}$$

where $u(k)$ is the unit step function, N is the round-off number at k_0+1 steps and $m=(J_s-J_t)/J_s$.

Comparing (16) with (17), it is observed that the step response of inertia compensation part of WTS (denoted by $\alpha_{wts}(k)$) can be decomposed into two response components. The first, called expected response and illustrated by the solid line in Fig. 4(a), is identical with that of inertia part of WT $\alpha_{wt}(k)$. The second is unexpected and defined as the deviation response $\alpha_d(k)$ which manifests as an exponential sequence. Similarly to the above stability condition, the convergence of $\alpha_{wts}(k)$ is determined by:

1) If $|m|<1$, i.e. $J_t / J_s < 2$, the $\alpha_d(k)$ converges to zero with time series and the $\alpha_{wts}(k)$ approaches the $\alpha_{wt}(k)$, as represented by the line marked with * in Fig. 4(a);

2) If $|m|>1$, i.e. $J_t / J_s > 2$, the $\alpha_d(k)$, as shown by the lines with different symbols in Fig. 4(b), is oscillatory and is periodically amplified by constant multiples at every k_0+1 steps. Consequently, $\alpha_{wts}(k)$, plotted by the grey dashed line in Fig. 4(a), oscillates with increasing amplitude on a 2(k_0+1) steps cycle.

In summary, the critical condition (i.e., $J_t / J_s < 2$) should be satisfied to maintain the WTS stability, and consequently the applicability of WTS is significantly limited.

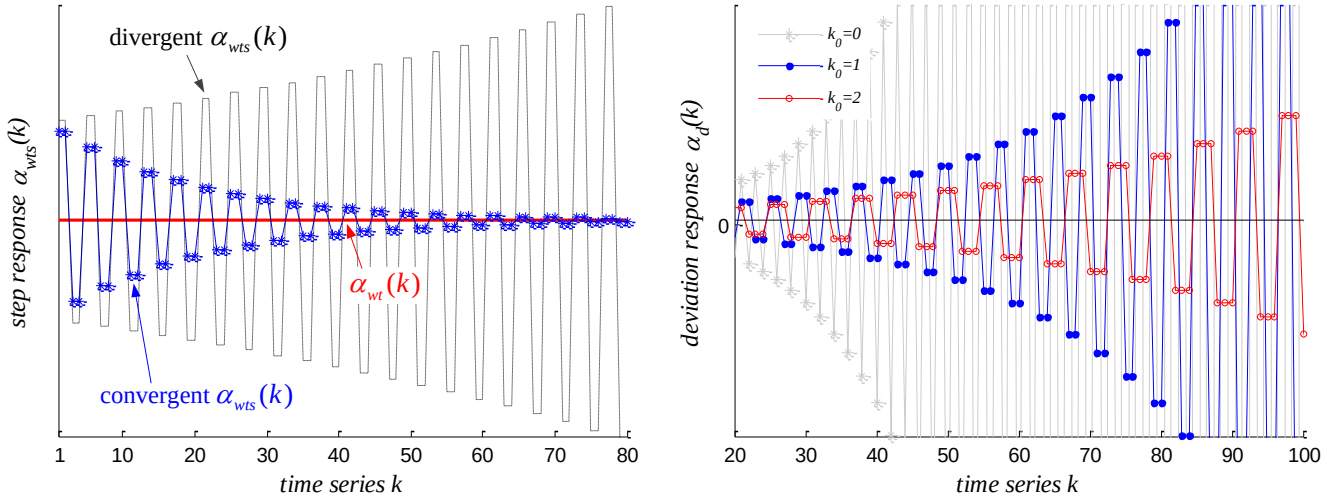

Fig. 4. *Step responses of inertia compensation part of WTS.*
(a) Convergence and divergence of the step response of inertia compensation part.
(b) Divergent deviation responses corresponding to the different time delay steps of communication.

4.2. Design of a high-order filter for deviation mitigation

It can be inferred from (16) that to improve the inertia compensation scheme, the deviation response component $\alpha_d(k)$ should be filtered away without changing the expected response component $\alpha_{wt}(k)$.

According to (16), the $\alpha_d(k)$ is a regular sequence amplified by constant multiples at every k_0+1 steps. Based on this law, a (k_0+1)th-order digital filter is designed to mitigate the divergent deviation in discrete time domain as follows:

$$c(k) = \alpha_f \cdot c(k - k_0 - 1) + \beta_f \cdot r(k) \tag{18}$$

where $r(k)$ is the input, $c(k)$ is the output, β_f is the gain coefficient, α_f is the (k_0+1) th-order coefficient of the filter. Note that the coefficients from first-order to k_0 th-order are set to zero since they do not contribute to deviation mitigation.

While filtering away the deviation response, the high-order filter should not modify the expected response $\alpha_{wt}(k)$. Therefore, the filter must satisfy the condition that

$$\text{when } r(k) = \alpha_{wt}(k),\ \lim_{k\to\infty} c(k) = \lim_{k\to\infty} \alpha_{wt}(k).$$

Then, (18) is rewritten as

$$\lim_{k\to\infty} c(k) = \alpha_f \cdot \lim_{k\to\infty} c(k - k_0 - 1) + \beta_f \cdot \lim_{k\to\infty} r(k). \tag{19}$$

Assuming $\lim_{k\to\infty} c(k - k_0 - 1) = \lim_{k\to\infty} c(k),$ it is obtained that:

$$\lim_{k\to\infty} \alpha_{wt}(k) = \alpha_f \cdot \lim_{k\to\infty} \alpha_{wt}(k) + \beta_f \cdot \lim_{k\to\infty} \alpha_{wt}(k). \tag{20}$$

Then, a constraint of coefficients of the filter is derived from (20):

$$\beta_f = 1 - \alpha_f. \tag{21}$$

Therefore, the expression of the filter can be rewritten as:

$$c(k) = \alpha_f \cdot c(k - k_0 - 1) + (1 - \alpha_f) \cdot r(k). \tag{22}$$

Using *z* transform, its frequency-domain expression is obtained:

$$G_f(z) = \frac{(1-\alpha_f) z^{k_0+1}}{z^{k_0+1} - \alpha_f}. \tag{23}$$

Then, as shown in Fig 5, the designed filter is added in the inertia compensation loop and transfer function of the inertia compensation part of WTS is modified as:

$$G'_{wts}(z) = \frac{z^{k_0+1} - \alpha_f}{J_s z^{k_0+1} - \alpha_f J_t + J_t - J_s} \tag{24}$$

which has (k_0+1) repeated poles in polar coordinates at

$$z_i^{k_0+1} = \frac{\alpha_f \cdot J_t - J_t + J_s}{J_s}, \quad i = 1, 2 \ldots k_0 + 1. \tag{25}$$

Compared with the previous poles determined by the inflexible structural parameters (J_s and J_t) in (15), these new poles are adjustable since the flexible coefficient α_f plays a role in location determination. When the poles of $G'_{wts}(z)$ fall inside the unit circuit in z plane, the inertia compensation part of WTS is stable and the corresponding time-domain response converges to the expected response $\alpha_{wt}(k)$.

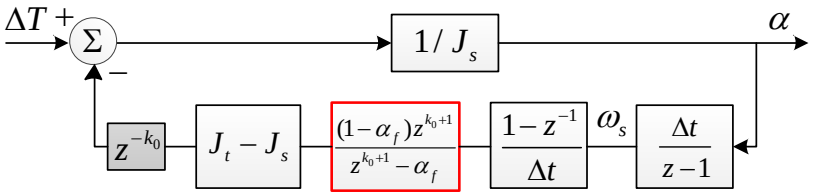

Fig. 5 *Inertia compensation part of WTS with (k_0+1)th-order filter added.*

Furthermore, the closer the poles are to the original point, the faster is the attenuation of oscillating deviation response in time domain. Therefore, the poles of $G'_{wts}(z)$ are assigned to the original point and the optimal value of α_f is then obtained:

$$\alpha_f^{opt} = (J_t - J_s) / J_t. \tag{26}$$

Accordingly, transfer function of the inertia compensation part in (24) is adjusted as:

$$G''_{wts}(z) = \frac{1}{J_s} - \frac{J_t - J_s}{J_t J_s} z^{-k_0 - 1}, \tag{27}$$

which remains a bit different from that of inertia part of WT

$$G_{wt}(z) = 1 / J_t, \tag{28}$$

because the effect of time delay cannot be eliminated instantly and completely. However, through the proposed high-order filter, the inertia compensation part of WTS system with time delay is stabilized and its time-domain response can rapidly converge to the expected response $\alpha_{wt}(k)$.

4.3. Response analysis of the inertia compensation part with the proposed filter

Performing the inverse z-transformation on (27) with a step input, the step response of inertia compensation part with the proposed filter added is obtained as:

$$\alpha'_{wts}(k) = \alpha_{wt}(k) + \alpha'_d(k) = \frac{1}{J_t} \cdot u(k) - \frac{(J_t - J_s)}{J_t J_s} \cdot [u(k) - u(k - k_0 - 1)]. \tag{29}$$

Compared with the unfiltered deviation response $\alpha_d(k)$ in (16), deviation response $\alpha'_d(k)$ modified by the proposed filter converges to zero regardless of the value of J_t / J_s because the term $[u(k)-u(k-k_0-1)]$ becomes zero when $k \geq k_0+1$. Therefore, as illustrated in Fig. 6, the step response $\alpha'_{wts}(k)$ deviates from the expected response $\alpha_{wt}(k)$ during the first k_0+1 steps and then coincides with $\alpha_{wt}(k)$. The effect of deviation response $\alpha'_d(k)$ during the first k_0+1 steps is acceptable because the time delay and the control cycle are short.

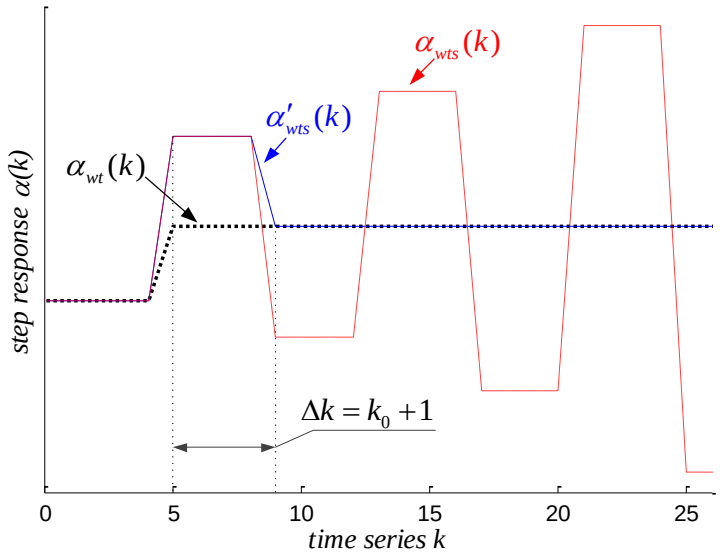

Fig. 6 *Step responses of inertia compensation part with/without the proposed filter.*

In addition, since a complex input can be regarded as a linear weighted combination of step signals, and inertia compensation part of WTS is a linear constant-coefficient system, the aforementioned step response analysis can be directly extended to the response of inertia compensation part excited by a complex input of imbalance torque. That is to say, a complex input of imbalance torque produces a bounded expected output of rotational acceleration accompanied with a deviation which is reduced to zero through the proposed filter after k_0+1 steps.

To sum up, through the improved inertia compensation scheme in which a (k_0+1)th-order filter is added, the deviation response is filtered away and the inertia compensation part of WTS not only becomes stable but also possesses acceleration properties similar to WT. Meanwhile, according to the optimum selection of parameter α_f in (26), a feasible ratio of J_t to J_s is

$$J_t / J_s = \frac{1}{1-\alpha_f}. \tag{30}$$

which indicates that the J_t / J_s for ensuring WTS stability is significantly increased as compared to the critical condition (i.e., $J_t / J_s < 2$) mentioned in Section 4.1 and thus more multiples of simulated moment of inertia can be stably compensated.

5. Experimental validation

In this section, a 15kW WTS-based WECS test bench (specifications as listed in Table 1) is built (Fig. 7(a)). Then, the improved inertia compensation scheme is verified by comparing with the current one that also employs a LPF but ignores the communication delay [5].

Table 1 The specification of the WTS-based WECS test bench

Description	Value
Rated power of IM	18.5 kW
Rated speed of IM	1500 rpm
Rated power of PMSG	15 kW
Rated speed of PMSG	1500 rpm
Moment of inertia of M-G set	0.72 kgm^2
Control cycle of PLC	20 millisecond
Resolution ratio of encoders	1024 pulse/round

5.1. System implementation of test bench

The WTS test bench built in the laboratory consists of:

1) A M-G set consisting of a three phase induction motor (IM) and a permanent magnet synchronous generator (PMSG);

2) ETS based on VACON industrial converters;

3) Real-time DCS based on Beckhoff Programmable Logic Controller (PLC); and

4) A host computer for user interface.

The detailed hardware configuration is shown in Fig. 7(b). The real-time DCS first generates the wind speed and computes the aerodynamic torque according to the aerodynamic model. Meanwhile, the rotational acceleration is observed by optical encoder and filtered to calculate the inertia compensation torque T_{comp}. Then the simulated torque reference T_s^{ref} is obtained and sent to the motor drive via Profibus-DP field bus. However, due to the time taken for data transmission, the received torque reference is delayed by about 60 milliseconds, which means the time delay step of communication k_0 is 3 since the control cycle of PLC Δt is set to 20 milliseconds. Besides, the electromagnetic torque of PMSG is calculated by:

$$T_g = k_{opt} \cdot \omega_g^2 \tag{31}$$

which is a commonly used control strategy for maximum power point tracking (MPPT) of wind turbines, known as the optimal torque (OT) control [17]. k_{opt} is the optimal torque gain.

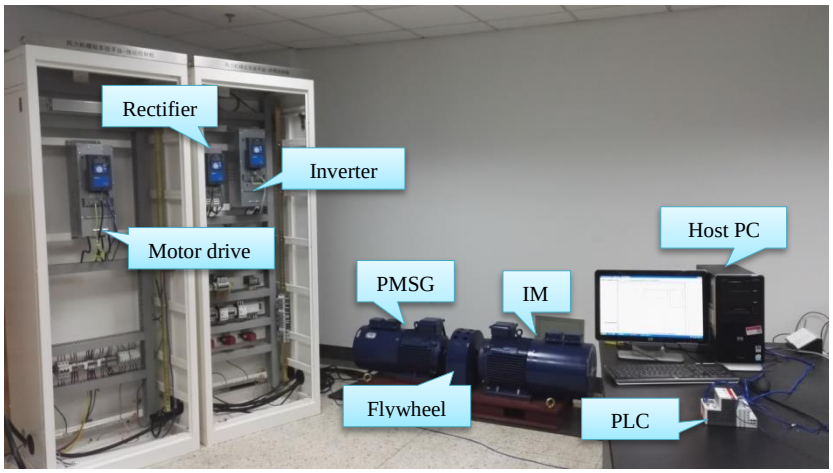

(a)

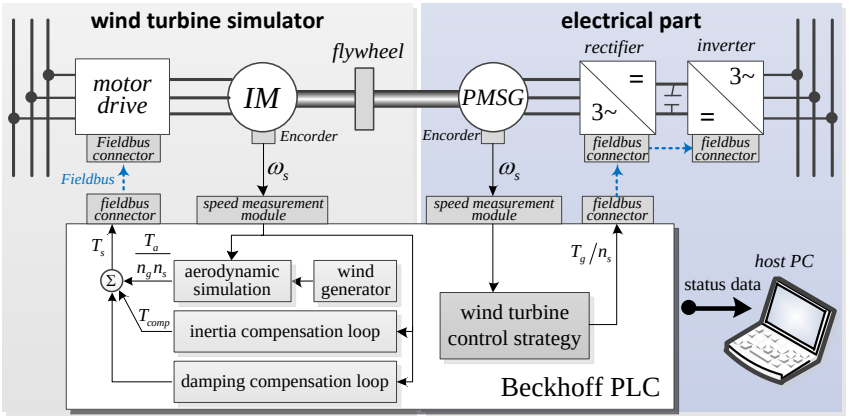

(b)

Fig. 7. *The WTS-based WECS test bench including M-G set and converters*
(a) Laboratory implementation for experimental testing.
(b) Schematic diagram of the WTS-based WECS test bench.

5.2. Necessity of considering communication delay

Without consideration of the communication delay, an inertia compensation scheme utilizing a first-order filter is proposed [5] and accordingly the stability boundary of a closed-loop WTS employing this scheme is theoretically derived as [5]:

$$J_t / J_s = \frac{2}{1-\alpha_f} \tag{32}$$

where α_f is the coefficient of the first-order filter. According to the time-domain response analysis of inertia compensation part of WTS mentioned in Section 4, the first-order filter, which is designed without

considering communication delay, cannot effectively filter away the deviation response. Therefore, it is reasonable to suppose that the obvious discrepancy between the stability boundary (32) (dotted line in Fig. 8(a)) and the one (thick solid line in Fig. 8(a)) obtained by trial-and-error experiments is mainly due to neglecting communication delay.

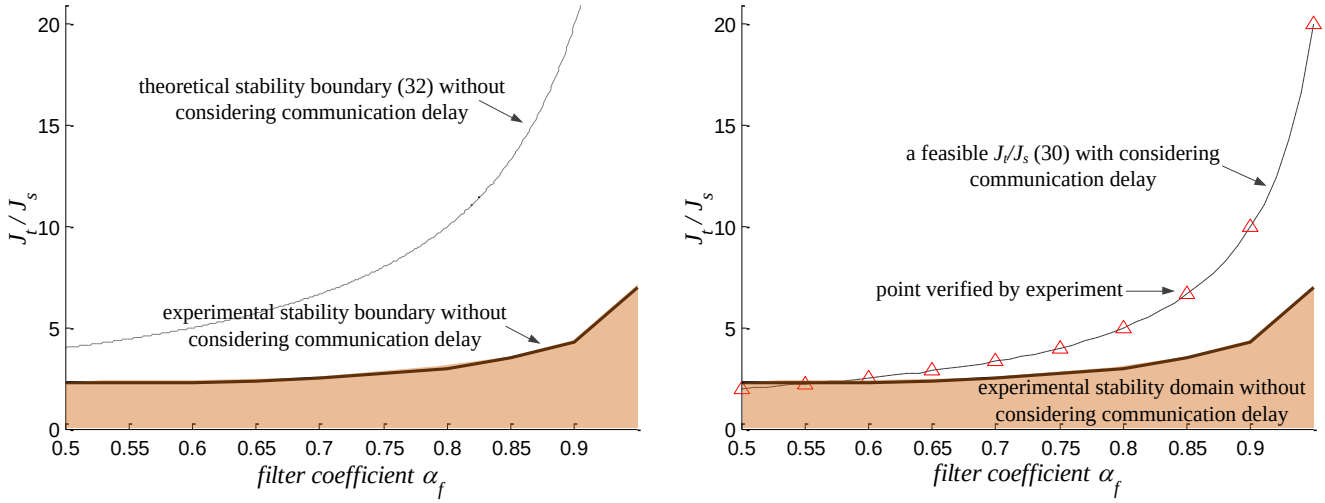

Fig. 8. *Experimental verification of the theoretical relationships between* J_t / J_s *and* α_f *.*
(a) The theoretical stability boundary (32) does not agree with the experimental one due to neglecting communication delay.
(b) A feasible $J_t / J_s - \alpha_f$ *curve obtained by the proposed inertia compensation scheme is experimentally verified by 10 points evenly chosen from the curve.*

Furthermore, in this paper, by fully considering the time delay in acceleration observation and communication, the WTS with the proposed inertia compensation scheme, in which a fourth-order filter corresponding to 3 steps of communication delay is employed, can stably operate on the $J_t / J_s - \alpha_f$ curve (dashed line in Fig. 8(b)) determined by (30). Moreover, 10 points marked with Δ are evenly chosen from this curve and experimentally validated. This indicates that when considering the communication delay, the theoretical result (30) agrees with the experimental result. Note that because high-order filter has more than one coefficient, this $J_t / J_s - \alpha_f$ curve only represents a subset of feasible J_t / J_s and α_f ensuring WTS stability rather than the stability boundary for the proposed scheme.

In addition, an unstable case of the WTS employing the conventional inertia compensation scheme without LPF (as mentioned in Section 4.1) is shown in Fig. 9(a). Note that the oscillating period of acceleration in experiments, measured as about 160 milliseconds, just agrees with the one derived from the time-delay model of inertia compensation part in Section 4.1, i.e. $2(k_0+1)$ steps of control cycle (k_0=3, Δt=20 milliseconds). This indicates that it is necessary to consider the communication delay in modelling of the inertia compensation part.

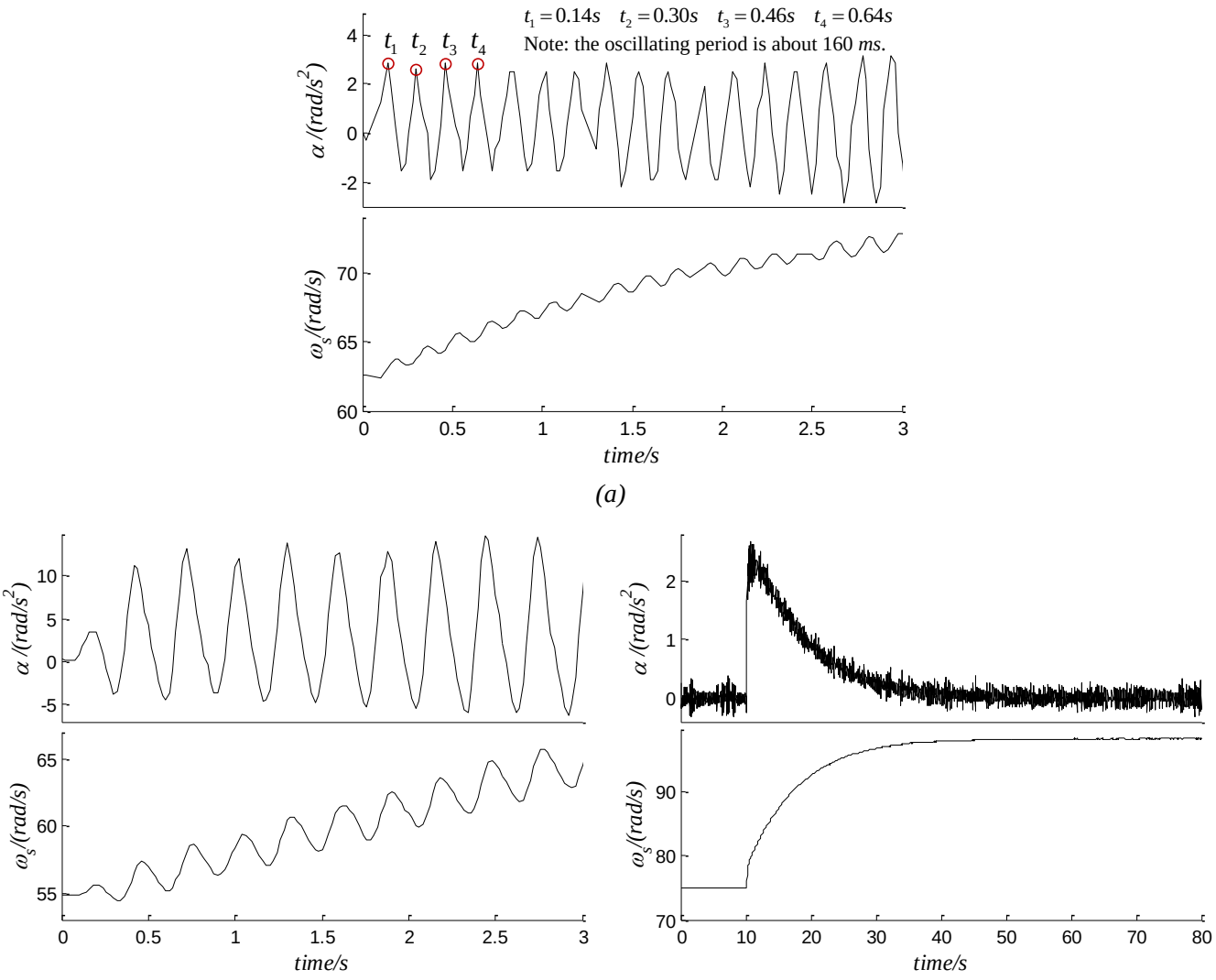

Fig. 9. *Experimental trajectories of the WTS employing the different inertia compensation schemes.*

(a) *Unstable trajectory of the WTS employing the conventional scheme without LPF ($J_t / J_s = 2.08$).*

(b) *Unstable trajectory of the WTS employing the scheme with the first-order filter ($J_t / J_s = 10.0$, $\alpha_f = 0.9$).*

(c) *Stable step response of the WTS employing the proposed scheme with the fourth-order filter ($J_t / J_s = 10.0$, $\alpha_f = 0.9$).*

5.3. Increase of the feasible J_t / J_s due to the proposed inertia compensation scheme

As shown in Fig. 8(b), when employing the inertia compensation scheme with the first-order filter, the feasible J_t / J_s for ensuring WTS stability should be chosen from the experimental stability domain without considering communication delay (shadow area). Even though α_d is set to 0.95, the maximum feasible J_t / J_s is about 7.0. Particularly, an unstable case of the WTS employing the inertia compensation scheme with the first-order filter ($J_t / J_s = 10.0$, $\alpha_f = 0.9$) is presented in Fig. 9(b).

In contrast, because the communication delay is considered and a high-order filter for filtering away the deviation response is developed, the feasible J_t / J_s is effectively increased by the proposed inertia compensation scheme, as indicated by the dashed line in Fig. 8(b). It can be seen that when α_f is set to 0.95, the feasible J_t / J_s is increased to 20. Particularly, Fig. 9(c) illustrates a stable step response of the WTS employing the proposed inertia compensation scheme with the fourth-order filter ($J_t / J_s = 10.0$, $\alpha_f = 0.9$).

5.4. Application of developed WTS

Firstly, experiments on MPPT control (OT control is assumed) of WTs with different inertia (J_t / J_s is set from 2 to 20 and correspondingly α_f is adjusted by (26)) under step wind speed and turbulence are conducted. As plotted in Fig. 10, rotational speed trajectory of each case shows that the WTS system always remain stable even when J_t / J_s is equal to 20. Moreover, the larger is the inertia the WT possesses, the slower the rotational speed tracks the maximum power point (MPP), which coincides with the conclusion that large inertia of WT leads to turbines' inability to accelerate or decelerate quickly in response to wind speed fluctuation [18]. Therefore, the inertia effect, especially the slow dynamic behaviour due to large inertia, is stably replicated by the WTS, applying the proposed inertia compensation scheme.

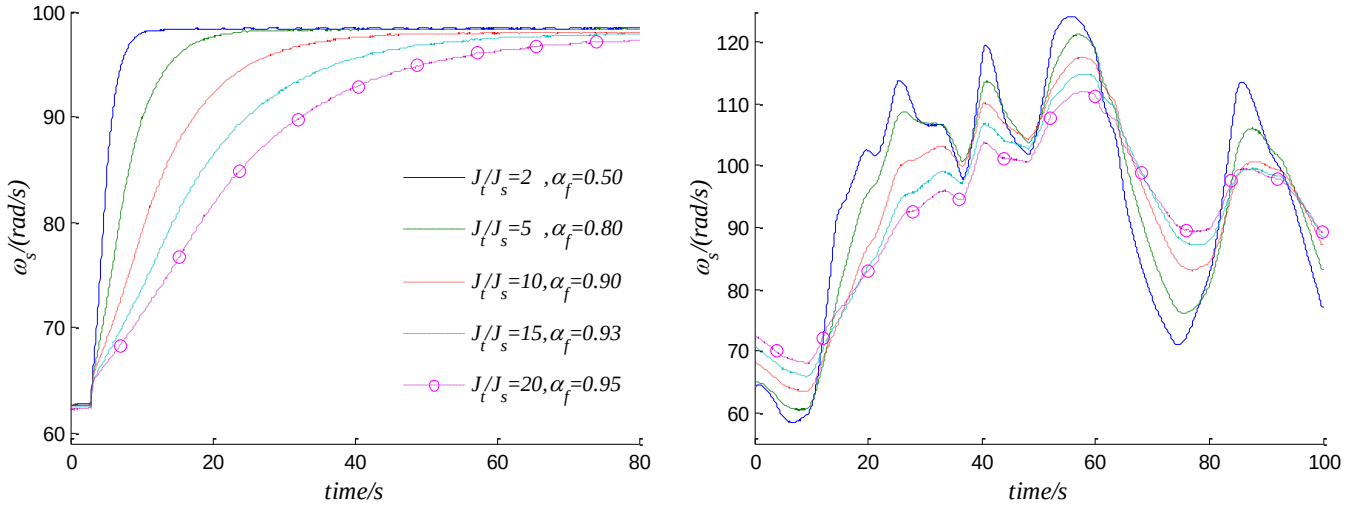

Fig. 10. *MPPT trials on the simulated WT with different moment of inertia.*
(a) step wind speed.
(b) turbulence.

Then, to comprehensively verify the applicability of the improved WTS, a 600kW CART3 wind turbine developed by NREL [13] is simulated by the WTS. Their characteristics are given in Table 2. It is

easy to see that because J_t/J_s (9.144) is close to 10, the dynamic behaviour of CART3 turbine can only be stably mimicked by the WTS applying the proposed inertia compensation scheme. Furthermore, the rotor speed trajectories of CART3 turbine operated by OT control in turbulence are compared in Fig. 11. They are respectively obtained by the WTS-based test bench and the FAST (Fatigue, Aerodynamics, Structures, and Turbulence) code [19] provided by NREL. As shown in Fig. 11, the similarity of two rotor speed trajectories demonstrates that the WTS developed in this paper can accurately reproduce the mechanical dynamics of CART3 turbine with large inertia.

Table 2 The characteristics of the WTS for emulating the CART3 wind turbine.

CART3 wind turbine		**WTS-based test bench**	
rated power	600.0 kW	rated power	15.0 kW
J_r	549206.4 kgm^2	J_s	0.72 kgm^2
J_g	34.4 kgm^2	n_s	50
n_g	43.165	J_t	6.584 kgm^2
J_w	329.2 kgm^2	J_t/J_s	9.144
D_w	0.0 N·m/rad·s	D_s	0.0263 N·m/rad·s

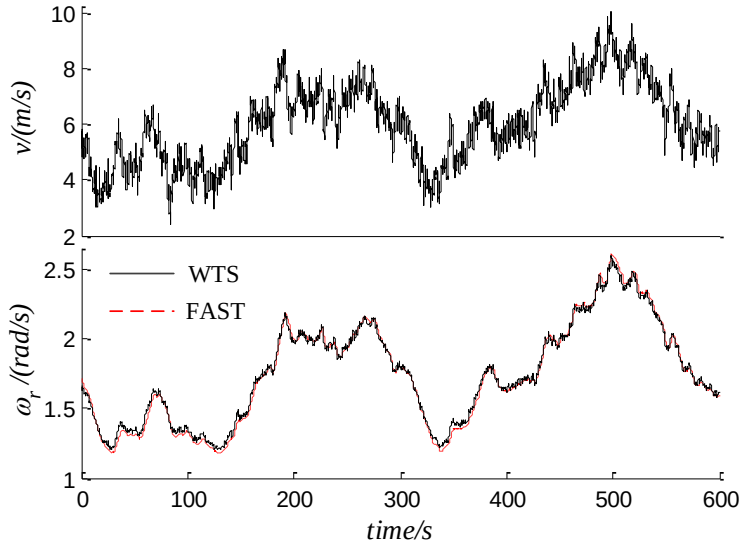

Fig. 11. *Comparison of rotor speed trajectories of CART3 turbine obtained by WTS-based test bench and FAST code.*

6. Conclusion

Because the slow dynamic behaviour of WT in response to turbulence caused by high rotor inertia exerts an important influence upon the design and operation of control strategies in WECS, the WTS should replicate a mechanical dynamics similar to the real WT. However, due to the instability of the WTS system caused by time delay of acceleration observation and command communication, the maximum inertia of WTs that can be stably emulated is significantly reduced and accordingly the applicability of WTS to simulating large-inertia WTs is greatly limited. To overcome the instability problem, the inertia compensation part is focused and extracted from WTS system and is then modelled as a linear difference

equation with consideration of time delay of acceleration observation and communication. Based on this model, by investigating the stability of the inertia compensation part, a high-order filter is added in the inertia compensation scheme to eliminate the deviation response caused by the time delay and stabilize the inertia compensation part. By employing the improved inertia compensation scheme, the feasible J_t / J_s for ensuring WTS stability is increased and thus the mechanical dynamics of large-inertia WT can be stably simulated by WTS system. The experimental results show that the WTS applying the proposed inertia compensation scheme can stably and accurately replicate the slow dynamic behaviour of the NREL CART3 wind turbine.

7. Acknowledgments

This work is supported by the National Natural Science Foundation of China (Grant No. 61673213, 51507080), the Perspective Research Foundation of Production Study and Research Alliance of Jiangsu Province of China (Grant No. BY2016004-13) and the Fundamental Research Funds for the Central Universities (Grant No. 30915011104).

8. References

[1] Bianchi, F. D., Mantz, R. J.: 'Wind turbine control systems. Principles, modelling and gain scheduling design' (Springer-Verlag Press, London, 2007)

[2] Boukhezzar, B., Siguerdidjane, H.: 'Nonlinear control of a variable-speed wind turbine using a two-mass model', IEEE Trans. Energy Convers., 2011, 26, (1), pp. 149–161

[3] Chang-Chien, L. R., Sun, C. C., Yeh, Y. J.: 'Modeling of wind farm participation in AGC', IEEE Trans. Power Syst., 2014, 29, (3) , pp. 1204-1211

[4] Li, W., Yin, M., Zhou, R., Jiang, M., Zou, Y.: 'Investigating instability of the wind turbine simulator with the conventional inertia emulation scheme'. Proc. ECCE2015, Montreal, Canada, September 2015, pp. 983-989

[5] Li, W., Yin, M., Chen, Z., Zou, Y.: 'An improved inertia compensation scheme for wind turbine simulator based on deviation mitigation', Journal of Modern Power System and Clean Energy, published online.

[6] Chen, J., Chen, J., Chen, R., Chen, Z., Gong, C., Yan, Y.: 'Static and dynamic behaviour simulation of wind turbine based on PMSM', Proceedings of the CSEE, 2011, 31, (15), pp. 40–46

[7] Chen, J., Chen, J., Gong, C., Wang, H.: 'Design and analysis of dynamic wind turbine simulator for wind energy conversion system'. Proc. 38th Annu. Conf. IEEE Ind. Electron. Soc., Montreal, Canada, October 2012, pp. 971-977

[8] Neammanee, B., Sirisumrannukul, S., Chatratana, S.: 'Development of a wind turbine simulator for wind generator testing', International Energy Journal, 2007, 8, (1), pp. 21-28

[9] Li, H., Steurer, M., Shi, K. L., Woodruff, S., Zhang, D.: 'Development of a unified design, test, and research platform for wind energy systems based on hardware-in-the-loop real time simulation', IEEE Trans. Ind. Electron., 2006, 53, (4), pp. 1144–1151

[10] Liu, Y., Zhou, B., Guo, H., Zhou, X., You, X.: 'Static and dynamic behaviour emulation of wind turbine based on torque PDF', Transactions of China Electrotechnical Society, 2014, 29, (11), pp. 116-125

[11] Guo H, Zhou B, Liu Y, Xu, E., You, X.: 'Static and dynamic behaviour emulation of wind turbine based on load torque observation', Proceedings of the CSEE, 2013, 33, (27), pp. 145–153

[12] Munteanu, I., Bratcu, A. I., Bacha, S., Bacha, S., Roye, D., Guiraud, J.: 'Hardware-in-the-loop-based simulator for a class of variable-speed wind energy conversion systems: Design and performance assessment', IEEE Trans. Energy Convers., 2010, 25, (2), pp. 564-576

[13] Darrow, P. J.: 'Wind turbine control design to reduce capital costs' (National Renewable Energy Laboratory, 2010)

[14] Sipahi, R., Niculescu, S. I., Abdallah, C. T., Sipahi, R., Michiels, W., Gu, K.: 'Stability and stabilization of systems with time delay, limitations and opportunities', IEEE Control Syst. Mag., 2011, 31, (1), pp. 38-65

[15] Loiseau, J. J., Michiels, W., Niculescu, S. I., Sipahi, R.: 'Topics in time delay systems: analysis algorithms and control', Lecture Notes in Control and Information Sciences., 2009, (388)

[16] Merry, R., van de Molengraft, M., Steinbuch, M..: 'Velocity and acceleration estimation for optical incremental encoders', Mechatronics, 2010, 20, (1), pp. 20–26

[17] Abdullah, M. A., Yatim, A. H. M., Tan, C. W., Saidur, R.: 'A review of maximum power point tracking algorithms for wind energy systems', Renew. Sustainable Energy Rev., 2012, 16, (5), pp. 3220–3227

[18] Tang, C., Soong, W. L., Freere, P., Pathmanathan, M., Ertugrul, N.: 'Dynamic wind turbine output power reduction under varying wind speed conditions due to inertia', Wind Energy, 2013, 16, (4), pp. 561–573

[19] Jonkman, J. M., Buhl Jr, M. L.: 'Fast user's guide' (National Renewable Energy Laboratory, 2005)